Occurrence of heat wave in Korea by the displacement of South Asian High

Yumi Cha
National Institute of Meteorological Sciences
JaeWon Choi
Busan National University: Pusan National University
Eung-Sup Kim
Pusan National University
Joong-Bae Ahn (jbahn@pusan.ac.kr)
Pusan National University https://orcid.org/0000-0001-6958-2801

Research Article

Keywords: South Asian high, heat wave days, circumglobal teleconnection pattern, Indian summer monsoon

Posted Date: April 26th, 2021

DOI: https://doi.org/10.21203/rs.3.rs-442109/v1

Abstract

The South Asian high (SAH) index was defined using the 200 hPa geopotential height for 1973–2019. Of movements of the SAH center in the north-south, east-west, northwest-southeast, and southwest-northeast directions, movement in the northwest-southeast direction showed the highest positive correlation with heat wave days (HWDs) in South Korea. Thirteen years with the highest SAH values (positive SAH years) and 13 years with the lowest SAH values (negative SAH years) were selected from a time series of SAH indices from which the linear trend was removed, and differences between these two groups were analyzed. An analysis of vertical meridional circulation averaged along 120°-130°E showed that in latitude zones containing Korea, anomalous downward flows with anomalous high pressures formed in the entire troposphere and coincided with positive air temperature and specific humidity. An analysis of stream flows and geopotential heights showed that in positive SAH years, anomalous anticyclones developed in Korea, the North Pacific, North America, western Europe, and the Iranian Plateau. These anticyclones had the wavenumber-5 pattern and showed more distinct barotropic vertical structure**s** at higher altitudes, which resembled the circumglobal teleconnection (CGT) pattern. The maintenance of CGT depends on the interaction between CGT circulation and the Indian summer monsoon (ISM), which has a major influence on the mid-latitude atmosphere. Strengthening of the ISM results in the formation of upper-level anomalous anticyclones in the northwestern Iranian Plateau and creates continuous downstream cells along the waveguide due to Rossby wave dispersion. When diabetic heating by Indian summer monsoon precipitation is strengthened, the SAH is strengthened to the northwest of India, and a positive CGT pattern is formed. As a result, anomalous anticyclones were formed in all layers of the Korean troposphere resulting in heat waves, tropical nights, and droughts exacerbated in South Korea.

1. Introduction

Heat wave is a period of extremely hot weather, but unfortunately, given the lack of a clear definition, heat wave has been defined in different ways in studies. Heat wave is one of the most dangerous natural disasters and is considered one of the major risk factors in South Korea that causes many casualties. Anderson and Bell (2009) reported that the number of deaths increased by approximately 3.0% within one day of a heat wave. For instance, more than 70,000 people died in 2003 when a record-breaking heat wave affected Europe (Robine et al. 2008; Schär et al. 2004), and 14,802 of these deaths occurred in France. During the period, the temperature in France exceeded 40°C on seven consecutive days (Fink et al., 2004; Garcia-Herrera et al., 2010). In Chicago, USA, about 600 people died over five days during a heat wave in 1995 (Klinenberg, 1999; Semenza et al., 1996), and in California, more than 140 people died between July 16 and 25, 2006 (Knowlton et al., 2009). In South Korea, it was reported around 3,400 people died from a heat wave in 1994 (Kysely and Kim, 2009).

According to future climate scenarios that address global warming, the frequencies, durations, and intensities of heat waves are going to increase due to changes in atmospheric circulation (Meehl and Tebaldi 2004; IPCC 2013). If greenhouse gas (GHG) emissions follow the current trend, heat wave days

(HWDs) will continue to increase globally and in Korea until the late 21st century (Kim et al. 2016). Furthermore, as maximum, minimum, and mean air temperatures increase, tropical night days (TNDs) are also expected to increase (Hulme et al. 1994; Choi et al. 2007; Ha et al. 2004; Kim et al. 2014; Lee and Kang 1997). Consequently, research on heat waves has been actively pursued to reduce their impacts and ensure adequate preparation.

Studies on heat waves in East Asia describe the role of convective activity in the subtropical monsoon region, but these descriptions were not accompanied by a specific explanation of the role of interannual or intraseasonal time-scale variations. Convective activities in the subtropical monsoon region related to the phase of El Niño/La Niña have continuous effects mostly during summer on an interannual timescale. However, the two primary modes (BSISO1 and BSISO2) of boreal summer intraseasonal oscillation (BSISO) moving north or northwest in the Asian monsoon region influence the generation of heat waves and heavy rainfall depending on their phase in the intraseasonal timescale (Hsu et al., 2016, 2017; Lee et al., 2017a; Lee et al. 2019).

Convective activities in the tropical and subtropical monsoon regions can influence heat waves and heavy rainfall events in mid-latitude through various teleconnections in a El Niño/La Niña phase-dependent manner (Ding et al., 2011; Lee et al., 2011, 2017b; Lee and Ha, 2015; Ha et al., 2018; Lee, 2018; Yeo et al., 2019; and many others). When convection is active in the western North Pacific monsoon region, a Western Pacific-North America (WPNA) teleconnection (or Pacific-Japan teleconnection) develops and the heat wave risk increases when an anticyclonic circulation anomaly develops in East Asia (or in the Kamchatka Peninsula region) (Ding et al., 2011). In the western North Pacific (WNP) and in the East Asian region, the Rossby wave spreads in a meridional direction, and Yeo et al. (2019) named this phenomenon ‘M-wave teleconnection.’ The western North Pacific summer monsoon (WNPSM) exhibits active variability in the summer when El Niño/La Niña disappears. In contrast, when convection is active in the Indian monsoon region, a circumglobal teleconnection (CGT) covering the entire northern hemisphere develops, which can increase the risk of heat waves in the East Asian region (Ding et al. 2011). When this happens, Rossby wave dispersion is dominant in the zonal direction, and hence, Yeo et al. (2019) named this ‘Z-wave teleconnection’. Furthermore, when El Niño disappears and La Niña develops, as occurred in the summers of 2010 and 2016, WPNA teleconnection and CGT can simultaneously influence heat waves in East Asia (Lee, 2018).

The studies on heat waves in Korea have been mainly conducted using case-centered designs (e.g., Kim et al. 1998; Byun et al. 2006). The atmospheric structure that causes heat waves in Korea has highly diverse spaciotemporal scales. From the perspective of large-scale atmospheric circulation, the representative cause of heat waves in Korea is abnormal expansion of the western North Pacific subtropical high (WNPSH). For example, heat waves were caused when the WNPSH, which had been heading north, settled near Korea under the influence of El Niño in 1987 and typhoon “Vanessa” in 1994 (Kim et al. 1998). Furthermore, in 2004, an abnormal high air temperature event occurred in Miryang, Korea when the axis of a warm area moved south due to WNPSH strengthening as heating in the continent was increased by reduced snow cover on the Tibetan Plateau and a secondary circulation

caused by a typhoon (Byun et al. 2006). Heat waves can also be caused in Korea by the orographic effect such as the Föhn phenomenon. When the easterly wind from the Young-Dong region in Korea causes a Föhn phenomenon, the Young-Seo region, west of the Taebaek Mountains, has high air temperature and low relative humidity (Lee 1994). And when a westerly wind appears in the Young-Seo region, a warm and dry atmosphere is formed in the Young-Dong region by a similar principle (Kim and Hong 1996).

Yeh et al. (2018) analyzed in more detail how two teleconnection patterns have influenced heat waves in Korea. First, in the subtropical WNP region, an anticyclonic circulation anomaly was induced in Mongolia and an anticyclonic circulation anomaly in the Kamchatka Peninsula induced by convective activity acted as blocking. Second, in the Indian monsoon region, anticyclonic circulation anomalies were maintained continuously in Mongolia and the Kamchatka Peninsula by the CGT pattern induced by active convection. Both effects strengthened the anticyclonic circulation anomaly in Mongolia and the Kamchatka Peninsula. Consequently, hot and dry northerly winds flowed into Korea at the upper level, which increased air temperature and caused heat waves.

In relation to the above studies, the present study analyzes changes in heat waves in Korea with respect to displacement of the South Asian high (SAH). In Sect. 2, data and methodologies are introduced, and in Sect. 3, the SAH index is defined. In Sect. 4, relationships between changes in Korean heat waves are examined according to SAH displacement, and the causes of these changes are investigated. Finally, Sect. 5 provides a summary of the study.

2. Data And Methodology

2.1 Data

This study used surface air temperatures (SATs), precipitations, and Palmer Drought Severity Index (PDSI) data obtained at 58 in-situ weather observation stations in South Korea. These data can be obtained from the website of the Korea Meteorological Administration (KMA) (https://www.kma.go.kr). Spatial distributions of the observation stations are presented in Fig. 1a, which shows stations evenly distributed around the country. Observational data of island such as Ullengdo and Jejudo were excluded from the study because they exhibit unique island weather characteristics. Data obtained after 1973 were used because the number of weather observation stations increased sharply after 1973. The HWD and TND data used in this study are accessible at the KMA website (https://data.kma.go.kr/climate/). The KMA defines HWD as the number of days when the daily maximum temperature is $\geq 33°C$, and TND as the number of days when the minimum temperature at night is $\geq 25°C$. Furthermore, since HWDs usually occur in July and August in Korea (Fig. 1b), July-August mean data were used in this study. In Korea, TNDs also mainly occur in July and August (not shown).

In this study, the East Asian summer monsoon (EASM) index (EASMI) derived by Li and Zeng (2002, 2003, 2005) was used. In addition, we used WNPSM and Indian summer monsoon indices (WNPSMI and ISM indices) provided by the Asia-Pacific data research center (APDRC) website of the University of Hawaii (http://apdrc.soest.hawaii.edu/projects/monsoon/seasonal-monidx.html). Indian Rainfall (AIR)

indices were provided by the Indian Institute of Tropical Meteorology (IITM) website (https://www.tropmet.res.in/Data%20Archival-51-Page).

Data of the Regional Specialized Meteorological Center (RSMC)-Tokyo Typhoon Center were used to analyze tropical cyclones (TCs). In addition, the National Center for Environmental Prediction/National Center for Atmospheric Research (NCEP/NCAR) Reanalysis dataset (Kalnay et al. 1996) was used to analyze large-scale environments and atmospheric circulation. Monthly global SST data used was obtained by Extended Reconstructed SST analysis (version 3) by the National Oceanic and Atmospheric Administration (NOAA) (Smith et al. 2008), and precipitation data were obtained from the Global Precipitation Climatology Project (GPCP) version 2.3 (Adler et al. 2003).

2.2 Methodology

The two-tailed Student's t-test was used to determine the significances of results (Wilks 1995).

A TC was defined as a TC that developed in the WNP above a tropical depression (TD). Extratropical cyclones (ECs) were included in the study because ECs are transformed from TCs and have caused considerable casualties and property damages in the mid-latitude regions in East Asia.

3. Definition Of South Asian High (Sah) Index

Figure 2a shows 200 hPa geopotential heights averaged over 47 years (1973–2019). Here, SAH is defined as a region larger than 12,500 gpm. The SAH is zonally stretched from the Arabian Peninsula to southern China and is located between latitudes 20° to 30°N. In this study, SAH centers were defined as: A-area (27.5°-32.5°N, 55°-75°E), B-area (27.5°-32.5°N, 85°-105°E), C-area (22.5°-27.5°N, 55°-75°E), and D-area (22.5°-27.5°N, 85°-105°E). Using averages of these four areas, we calculated differences between east (BD-area) and west (AC-area) areas, south (CD-area) and north (AB-area) areas, southwest (C-area) and northeast (B-area) areas, and northwest (A-area) and southeast (D-area) areas.

Using these four sets of SAH values, we examined correlations between the movements of SAH center in the east-west, south-north, southwest-northeast, and northwest-southeast directions and Korean HWDs (Table 1). The strongest correlation with a positive correlation coefficient of 0.62, occurred when the SAH center moved in a northwest-southeast direction, and this correlation was significant at the 99% confidence level.

Table 1
Correlation between each displacement of South Asian high (SAH) and heat wave days (HWD) in Korea.

	Displacement of South Asian high (SAH)			
	A minus D	B minus C	AB minus CD	BD minus AC
Heat wave days (HWD)	0.62	-0.04	0.51	-0.40

In addition, movements of the SAH center in a south-north direction or an east-west direction exhibited correlations of 0.51 and − 0.40, respectively, and both correlations were significant at the 99% confidence level. However, when the SAH center moved in a southwest-northeast directions the correlation was negative and non-significant. Therefore, we investigated the relationship between movement of the SAH center in the southeast-northwest direction and HWDs in Korea, which had the strongest correlation. SAH indices represent the movement of the SAH center in a northwest-southeast direction and were calculated as follows (Wei et al. 2012; Wei et al. 2014):

$$\text{SAH index} = \text{Z200(A)}_{(27.5-32.5\text{N},55-75\text{E})} - \text{Z200(D)}_{(22.5-27.5\text{N},85-105\text{E})}$$

As shown in Fig. 2b, this index is defined as a normalized value of the area-mean 200 hPa geopotential height difference between A-area and D-area. Thus, a positive (negative) index means that the SAH center is strengthened in the northwest (southeast).
Figure 2b shows the time series of HWDs and SAH indices in Korea calculated using the above equation. Both time series exhibited interannual and interdecadal variations, showed an obvious in-phase relationship, and were positively correlated at 0.62, which was significant at the 99% confidence level. These results imply that when SAH is strengthened in the northwest direction, HWDs increase in Korea. Meanwhile, the SAH index tended to increase weakly. However, when the linear trend is removed from a SAH index time series, the correlation changes. Thus, we removed the linear trend from the SAH index time series and reanalyzed the correlation between the two variables (Fig. 2c). A high positive correlation of 0.60 was obtained, which was similar to that of the original correlation, and this correlation was also significant at the 99% confidence level. Therefore, we selected 13 years with highest SAH indices and removed the linear trend (hereinafter referred to as ‘positive SAH years’) and 13 years with the lowest SAH indices and removed the linear trend (hereinafter referred to as ‘negative SAH index’) (Table 2). These selected 26 years accounted for about 56% of the total analysis period. During positive (negative) SAH years, the SAH center was strengthened in the northwest (southeast) directions. Among positive SAH years, HWDs were < 10 days in two (1976, 2011), whereas among negative SAH years, HWDs were ≤ 10 days in five years (1983, 2000, 2010, 2015, and 2019). Consequently, the average HWD of positive SAH years was 15.8 days, and the average HWD of negative SAH years was 7.7 days, and this difference of 8.1 days was significant at the 95% confidence level. Next, this study analyzes the difference between the average of the positive SAH years and the average of the negative SAH years in the following section.

Table 2
Statistics on HWD in Korea in positive and negative SAH years.

Positive SAH years		Negative SAH years	
Year	HWD	Year	HWD
1973	16.2	1979	5.9
1976	3.4	1982	8.8
1978	17.0	1983	11.3
1984	13.4	1986	5.7
1985	15.2	1987	2.1
1994	31.1	1989	4.7
1995	11.8	1991	3.8
1997	12.8	1993	0.1
2001	12.7	2000	12.4
2006	14.4	2010	13.9
2011	7.5	2014	7.4
2013	18.5	2015	10.1
2018	31.5	2019	13.8
Average	15.8	Average	7.7

4. Differences Between Positive And Negative Sah Years

4.1 Spatiotemporal variations of SATs and precipitation in Korea

During positive SAH years, most areas, excluding the northeastern region of Korea, had SATs of ≥ 25°C (left panel of Fig. 3a), whereas during negative SAH years, most regions had SATs of ≤ 24°C (left panel of Fig. 3b). Differences between the two groups showed warm anomalies in most regions, though largest warm anomalies appeared along the coast (left panel of Fig. 3c). The time series of the difference in daily SATs between the two groups show a strong warm anomaly from July to early September, which suggested a high probability of a heat wave in Korea in positive SAH years (left panel of Fig. 3d). During other seasons, SAT values were higher in negative SAH years.

Regarding precipitation, the northern region of Korea experienced large precipitations of > 320 mm during positive SAH years, whereas the southern and eastern coasts experienced precipitations of ≤ 240 mm

(right panel of Fig. 3a). During negative SAH years, large precipitations of ≥ 320 mm were distributed in the southern region (right panel Fig. 3b). As a result, differences between the two groups showed a negative anomaly in the southern and eastern regions and a small positive anomaly in the northern region (right panel Fig. 3c). This result was associated with a high warm SAT anomaly along the coast of Korea. In other words, during positive SAH years, SAT increased and precipitation decreased because of many clear days in coastal regions. The time series of differences in daily precipitation between the two groups show strong negative anomalies from early July to September (right panel ofFig. 3d), which were associated with the appearance of a warm SAT anomaly. In other words, the probability of a heat wave was increased by low precipitation during this period.

4.2 Large-scale environments

To examine the spatial distributions of SAHs in the positive and negative SAH years, average 200 hPa geopotential height was analyzed in both (Fig. 4). During positive SAH years, the 12,560gpm contour was located from Iran to northern India (Fig. 4a), but during negative SAH years, it was distributed more broadly in the east-west direction from northeast of the Arabian Peninsula to the Tibetan Plateau (Fig. 4b). Thus, during positive SAH years, SAH center was located at 30°N, 58°E, whereas during negative SAH years, was located at 27°N, 93°E, which means during positive SAH years, the SAH was located more to the northwest.

We also examined the spatial distribution of regression of 2m air temperature (Air2m) against SAH indices (Fig. 5a). Positive values were observed from the central region of China to Korea and for all Japan. Furthermore, positive values also appeared in the Central Asia and North Pacific regions at 40°-50°N, which means that when the SAH is strengthened in the northwest, Air2m increased in this region. Therefore, when the SAH is strengthened in the northwest region, there is a possibility that a heat wave could be generated in Korea, central China, and Japan. Thus, we divided the East Asian region into northeast Asia (30°-40°N, 120°-130°E) and South China (20°-25°N, 100°-120°E) and analyzed the correlation between Air2m averaged for each region and SAH indices with the linear trend removed. SAH indices and the time series of Air2m averaged for northeast Asia showed a clear in-phase relationship (Fig. 5b) with a positive correlation of 0.58, which was significant at the 99% confidence level. This means that when the SAH strengthened in a northwest (southeast) direction, Air2m increased (decreased) in northeast Asia. A clear out-of-phase relationship was observed between SAH indices and the Air2m time series averaged for South China (Fig. 5c) with a significant negative correlation of -0.47, which was significant at the 99% confidence level. This means that when the SAH strengthened to the northwest (southeast), Air2m decreased (increased) in South China.

We then analyzed differences in specific humidity between the two groups. 850 hPa specific humidity exhibited a spatial distribution with a wave train shape, that is, a negative anomaly in the Arabian Peninsula, a positive anomaly in the northwestern region of India, a negative anomaly in west China, and a positive anomaly from central China to Korea and Japan (Fig. 6a). However, this spatial distribution weakened at higher altitudes (Figs. 6b and 6c). During positive SAH years, it might be expected that the discomfort index would be high because Air2m and specific humidity were high in northeast Asia.

Group differences in vertical meridional circulation averaged along 120°-130°E, which includes Korea, were also analyzed (Fig. 7a). Anomalous high pressures and downward flows were formed in 25°-35°N and distributed in 30°-35°N, which also contains South Korea. Therefore, during positive SAH years, a favorable environment existed for heat wave generation because anomalous high pressure was present in all layers of the Korean troposphere. Furthermore, positive anomalies of air temperature and specific humidity were distributed in 30°-50°N with centers located in 30°-40°N (Figs. 7b and 7c). As mentioned above, warm anomalies formed in all layers of the troposphere in Korea as a result of strengthened anomalous downward flows in all troposphere layers. In addition, due to positive strengthening of specific humidity in all layers of the troposphere, an environment was formed that favored a high discomfort index in Korea.

WNPSH is also associated with heat waves, and thus, we examined the spatial distributions of SAH and WNPSH in the two groups (Fig. 8). During positive SAH years, the SAH was located in 20°-40°N in a south-north direction and extended from Japanese eastern waters toward the east in the zonal direction (Fig. 8a). The WNPSH extended to the Shandong Peninsula in the northwest direction, and as a result, the two high pressure systems overlapped in Korea. This is consistent with the above result that during positive SAH years, the anomalous high strengthened in all layers of the Korean troposphere. Hence, during positive SAH years, the HWD can increase more in Korea, whereas during negative SAH years, the SAH develops more to the southeast, and the WNPSH extends to the southwest (Fig. 8b), which results in an overlap of the two high pressure systems in southern China. This means that the air temperature is likely to increase in South China during negative SAH years, which is consistent with the above result that in southern China SAH index and Air2m are negatively correlated.

4.3 Tropical cyclone activity

Frequent TCs can temporarily lower heat wave frequencies, and thus, we investigated differences in TC passage frequencies (TCPFs) between the two groups (Fig. 9). During positive SAH years, TCs show a strong tendency to move from the northeastern region of the Philippines to central China and then to northern China. As found above, this occurs because the WNPSH develops in the northwestern direction to the Shandong Peninsula during positive SAH years, whereas during negative SAH years, TCs mainly move from the far eastern sea of the Philippines to the East China Sea (ECS) and then to Korea and Japan, or to the west toward the Indochina Peninsula. As shown above, because the WNPSH develops in the southwest direction to South China during negative SAH years, TCs move toward the Indochina Peninsula, or even if they moves to the mid-latitude region of East Asia, it does not move more to the west, but moves to the northeast along the mid-latitude westerlies. Hence, during positive SAH years, HWDs can increase in Korea due to the low TC frequencies.

4.4 The relationship between HWDs in Korea and Circumglobal Teleconnection

Results of an analysis of differences in 850, 500, and 200 hPa stream flows and geopotential heights in the two groups are shown in Fig. 10. In general, during positive SAH years, anomalous anticyclones developed in Korea, the North Pacific, North America, Western Europe, and the Iranian Plateau. These anticyclones displayed the wavenumber-5 pattern and a barotropic vertical structure, which became more

distinct at higher altitudes. This spatial distribution is similar to the circumglobal teleconnection (CGT) pattern discovered by Ding and Wang (2005; 2011), who suggested that maintenance of the CGT depends on the interaction between CGT circulation and the ISM, which has a major influence on the mid-latitude atmosphere. A strengthened ISM forms an upper-level anomalous anticyclone in the northwestern region of India and generates continuous downstream cells along the waveguide through Rossby wave dispersion.

Thus, the ISM has a major effect on the CGT pattern, and therefore, we analyzed differences between precipitations in the two groups (Fig. 11). During positive SAH years as compared with climatology (meaning averages for July and August for 1973–2019), a negative anomaly was formed from the southwest to the northeast from the northeastern region of India to Central China and then to Korea and Japan (Fig. 11a). On the other hand, a positive anomaly was formed in the Indochina Peninsula, the South China Sea (SCS), and the eastern region of the Philippines. The spatial distribution of the difference between negative SAH years and climatology revealed a pattern opposed to that shown in Fig. 11a (Fig. 11b). The pattern correlation between the two spatial distributions was 0.88. The spatial distribution of Fig. 11a can be seen more clearly in the spatial distribution of the difference between positive and negative SAH years (Fig. 11c), and show that in Korea, decreased precipitations can increase HWDs. In contrast, the Indian subcontinent showed a positive anomaly. During positive SAH years, the negative anomaly of precipitation formed from Central China to Korea and Japan might mean weakening of the EASM, whereas a positive anomaly of precipitation formed in the eastern region of the Philippines might be associated with strengthening of the WNPSM. Therefore, we analyzed the time series for HWDs in Korea and for EASM and WNPSM indices (Figs. 11d and 11e). An obvious out-of-phase relationship was observed between HWDs and EASM indices (Fig. 11d), but a clear in-phase relationship was observed between HWDs and WNPSM indices (Fig. 11e). Consequently, the correlation between HWDs and EASM indices was significant and negative (correlation − 0.48), and that between HWDs and WNPSM indices was significant and positive (correlation − 0.51) at the 99% confidence level. This means that in Korea, an increase (decrease) in HWDs was associated with weakening (strengthening) of the EASM and strengthening (weakening) of the WNPSM.

According to Ding and Wang (2005; 2011), the effect of diabatic heating due to ISM precipitation maintains a center of action in the northwestern region of India. Therefore, we defined the CGT index as 200 hPa geopotential height averaged for the northwestern region of India (35°-50°N, 60°-70°E), and then analyzed the correlation between the SAH and CGT indices (Fig. 12a). The time series of these two indices represented interannual and interdecadal variations and showed a strong in-phase tendency and a positive correlation of 0.51, which was significant at the 99% confidence level. This implies that when the SAH is strengthened in the northwest (southeast), the CGT pattern is developed (weakened). Therefore, the time series of HWDs in Korea and CGT, ISM, and all Indian rainfall (AIR) indices were analyzed (Figs. 12b, 12c, and 12d). CGT, ISM, and AIR indices all showed in-phase relationships with HWDs in Korea with significant positive correlations of 0.60, 0.53, and 0.51 at the 99% confidence level, respectively. This means that HWDs increase (decrease) in Korea when the effect of the diabetic heating

by ISM precipitation is strengthened (weakened) and that CGT, ISM, and AIR are strengthened (weakened).

The correlation between HWDs in Korea and Air2m was also analyzed because the diabetic heating effect of ISM precipitation maintains a center of action located to the northwest of India (Fig. 13a). In general, correlations showed a pattern similar to the spatial distribution of the regression of Air2m against SAH index analyzed above. The pattern correlation between the two spatial distributions exhibited a positive correlation of 0.72, which occurred because HWDs in Korea and SAH indices showed the highest positive correlation (0.62) in northeast Asia. Furthermore, a positive correlation was also observed in the northwestern region of India. Therefore, the time series of HWDs in Korea and Air2m averaged for the northwestern region of India (area-A in Fig. 13a; 30°-40°N, 70°-80°E) were analyzed (Fig. 13b). These two variables showed a strong increasing trend, and a distinct in-phase relationship, and thus, a significant positive correlation of 0.48 at the 99% confidence level. This means that HWDs in Korea are strongly correlated with ISM variation and resulting CGT patterns.

4.5 Relationships between TNDs and PDSIs in Korea and SAH and CGT

We examined relations between the time series of TNDs in Korea and SAH and CGT indices (Figs. 14a and 14b). The time series of TNDs and SAH indices showed an increasing trend, particularly after 2010 (Fig. 14a) and a strong in-phase tendency, which resulted in a significant positive correlation of 0.60 at the 99% confidence level. TNDs and CGT indices also showed a distinct in-phase relationship (Fig. 14b) resulting in a positive correlation of 0.54 at the 99% confidence level, which suggests like HWDs, TNDs are also strongly correlated with ISM variations and resulting CGT patterns.

The higher the frequency of heat waves, the less the precipitation and the worse droughts can develop. Therefore, we examined relations between the time series of PDSI in Korea and SAH and CGT indices (Figs. 14c and 14d). PDSI time series and SAH indices showed a trend of worsening drought, particularly after 2010 (Fig. 14c) and a distinct out-of-phase relationship, which resulted in a significant negative correlation of -0.43 at a 99% confidence level. Furthermore, the correlation between PDSI and CGT indices also showed a distinct out-of-phase relationship (Fig. 14d), and a negative correlation of -0.41 at the 99% confidence level. These results indicated that not only HWDs and TNDs but also PDSIs were strongly correlated with ISM variations and resulting CGT patterns.

In addition, we investigated the difference in SST between the two groups (Fig. 14e). Analysis showed eastern Pacific (EP) La Niña in general, the cause of which requires further investigation. In particular, the sea areas around Korea and Japan showed strong warm anomalies, possibly because of a strong anomalous anticyclone in this region, low precipitation, and an increase in solar radiation. This strong warm anomaly that appears in the sea areas near Korea can increase the discomfort index by providing heat and moisture to coastal areas of Korea.

4.6 Extreme case analysis

Years of the highest and lowest frequencies in the HWD time series were selected, and the above results were analyzed for these two years (Fig. 15). The highest and lowest HWD frequencies occurred in 2018

and 1993, respectively. To examine the unique characteristics of these two years, the differences between climatology and these two years were analyzed. First, Air2m values in 2018 showed a warm anomaly from the Iranian Plateau and the northern region of India to Central China, Korea, and Japan (left panel Fig. 15a), which was similar to the pattern of the above regression of Air2m against the SAH index. The pattern in 1993 was the near opposite of that in 2018 and showed a cold anomaly in the 30°-50°N region (right panel Fig. 15a). The correlation between these two patterns showed a negative correlation of -0.52. Precipitation in 2018 showed a negative anomaly from west to east from the northern region of India to Central China, Korea, and Japan (left panel Fig. 15b), but a positive anomaly in India, the Indochina peninsula, the South China Sea (SCS), and the eastern sea of the Philippines, which resembled the results presented above regarding precipitation differences between the two groups. The pattern observed in 1993 exhibited a spatial distribution opposite to that observed in 2018, and the pattern correlation between these two spatial distributions had a negative correlation of -0.77 (right panel Fig. 15b). The SST in 2018 shows central Pacific (CP) El Niño in general, and a warm anomaly from west to east from the sea near Korea to the North American western sea (left panel of Fig. 15c). This latter case resembled SST differences between the two groups. In 1993, EP El Niño appeared in general, and a cold anomaly was observed in the west to east direction from seas near Korea and Japan to the north Pacific region. The pattern correlation between these two spatial distributions showed a negative correlation of -0.43. In the case of 200 hPa stream flows in 2018, anomalous anticyclones existed in Korea, North Pacific, North America, Western Europe, and the Iranian Plateau (left panel of Fig. 15d). This spatial distribution was similar to the spatial distribution of the difference in the 200 hPa stream flows between the two groups. Furthermore, the spatial distribution in 1993 was the opposite of that observed in 2018 (right panel of Fig. 15d). Thus, the two spatial distributions showed a negative pattern correlation of -0.75. TC tracks did not influence Korea in 2018 because TCs moved from the eastern sea of the Philippines to Central China and northern or southern China (left panel of Fig. 15e), which is similar to that observed for TCPF differences between the two groups. However, in 1993, TCs had a substantial impact on Korea (right panel of Fig. 15e).

5. Summary And Conclusions

SAH indices were defined using the 200 hPa geopotential height average for 1973–2019, and SAH centers were defined using four areas: A-area (27.5°-32.5°N, 55°-75°E), B-area (27.5°-32.5°N, 85°-105°E), C-area (22.5°-27.5°N, 55°-75°E), and D-area (22.5°-27.5°N, 85°-105°E). Using each of these four area-averaged 200 hPa geopotential height, the differences between the east (BD-area) and west (AC-area) areas, between the south (CD-area) and north (AB-area) areas, between the southwest (C-area) and northeast (B-area) areas, and between the northwest (A-area) and southeast (D-area) areas were obtained. Using these four differences, we examined correlations between the movements of the SAH center in the east-west, south-north, southwest-northeast, and northwest-southeast directions and HWDs in Korea. The strongest correlation was found when the SAH center moved in the northwest-southeast direction, and thus, the SAH index was defined as the difference between 200 hPa geopotential heights in the northwest and southeast regions.

We selected 13 years with a high SAH index with linear trend removed (positive SAH years) and 13 years with a low SAH index with linear trend removed and then analyzed differences between the averages of positive and negative SAH years. Firstly, we analyzed spatial distributions of regression of Air2m against SAH indices. Positive values were observed from Central China to Korea and Japan, and thus, the East Asian region was divided into Northeast Asia and South China, and then the correlation between SAH indices and Air2m averages was analyzed in each area. SAH indices and Air2m averages for Northeast Asia were positively correlated, meaning that when SAH strengthened (weakened) to the northwest, Air2m in northeast Asia increased (decreased). On the other hand, a negative correlation was observed between SAH indices and Air2m averages for South China.

Next, differences in specific humidity between the two groups were analyzed. A spatial distribution of wave train shape was observed, that is, a positive anomaly in the northwestern region of India, a negative anomaly in West China, and a positive anomaly from Central China to Korea and Japan. It is considered the discomfort index was extremely high during positive SAH years in northeast Asia, including Korea, due to high Air2m and specific humidity.

We also analyzed the difference in vertical meridional circulation averages along 120°-130°E, in which Korea is located. At 25°-35°N, anomalous high pressures and anomalous downward flows were formed, and their centers were distributed in 30°-35°N, which also contains South Korea. This indicated that during positive SAH years, there was a favorable environment in which the heat waves could increase because high pressures were present in all layers of the Korean troposphere. Furthermore, positive anomalies of air temperature and specific humidity were distributed in 30°-50°N, and their centers were in 30°-40°N.

The spatial distributions of SAH and WNPSH were examined in the two groups. First, during positive SAH years, the SAH was located in 20°-40°N in the meridional direction and extended to the eastern waters of Japan in the zonal direction. The WNPSH extended to northwest of the Shandong Peninsula. As a result, the two high pressure systems overlapped in Korea. During negative SAH years, the SAH extended more to the southeast than in positive SAH years, and the WNPSH extended to the southwest, and as a result, the two high pressure systems overlapped in South China.

Analysis of TCPF differences between the two groups showed that during positive SAH years, TCPFs showed a strong trend to move from the northeastern region of the Philippines to Central China and then to northern China. As shown by the analysis above, this occurred because, during positive SAH years, the WNPSH developed northwest of the Shandong Peninsula. By contrast, during negative SAH years, the WNPSH moved from the far east sea of the Philippines to the ECS and then to Korea and Japan or the Indochina Peninsula in the west. This occurred because during negative SAH years, the WNPSH developed in the south-west direction towards South China. Even though TCs moved toward the Indochina Peninsula or to the middle latitude region of East Asia, they did not move further to the west and moved to the northeast along mid-latitude westerlies. Consequently, HWDs increased during positive SAH years due to the low frequency of TCs in Korea.

Differences in stream flows and geopotential heights between the two groups were also analyzed. In general, during positive SAH years, anomalous anticyclones developed in Korea, the North Pacific, North America, Western Europe, and the Iranian Plateau. These anticyclones show the wavenumber-5 pattern and a barotropic vertical structure that became more distinct at higher altitudes. This spatial distribution was similar to the CGT pattern discovered by Ding and Wang (2005; 2011) (Fig. 16), who suggested that maintenance of CGT patterns depends on the interaction between CGT circulation and the ISM, which has a major effect on the mid-latitude atmosphere. ISM strengthening generates an upper-level anomalous anticyclone in the northwestern region of India and a continuous downstream of cells along the waveguide through Rossby wave dispersion. In short, the ISM substantially influences CGT patterns. Accordingly, we analyzed differences in precipitation between the two groups. A negative anomaly was formed from southwest to northeast from the northeastern region of India to Central China and then to Korea and Japan, whereas a positive anomaly was formed in the Indochina Peninsula, SCS, and the eastern Philippines. In contrast, the Indian subcontinent showed a positive anomaly. During positive SAH years, a negative anomaly formed from Central China to Korea and Japan implying EASM weakening, and a positive anomaly formed in the eastern Philippines and was associated with WNPSM strengthening.

According to Ding and Wang (2005; 2011), the effect of diabatic heating of ISM precipitation maintains the center of action in the northwestern region of India. Therefore, the CGT index was defined by the 200 hPa geopotential height averaged for the northwestern region of India, and the correlation between SAH and CGT indices was analyzed. These two variables showed a positive correlation of 0.51, meaning that when SAH strengthened to the northwest (southeast), the CGT pattern developed (weakened). Therefore, correlations between the time series of HWDs in Korea and CGT, ISM, and AIR indices were analyzed. They showed positive correlations of 0.60, 0.53, and 0.51, respectively, which meant that HWD in Korea increased (decreased) when the effect of diabetic heating due to ISM precipitation strengthened (weakened), and that CGT patterns and the ISM strengthened (weakened) and AIR increased (decreased).

In this study, we analyzed correlations between TNDs in Korea and SAH and CGT indices. TNDs and SAH or CGT indices showed positive correlations of 0.60 and 0.54, respectively. This suggests that TNDs like HWDs are strongly correlated with ISM variations and resulting CGT patterns.

The higher the heat wave frequency, the lower the precipitation, and the worse droughts can occur. Therefore, we analyzed correlations between PDSIs in Korea and SAH or CGT indices. PDSIs and SAH or CGT indices showed negative correlations of -0.43 and − 0.41, respectively, which suggested that like HWDs and TNDs, PDSI was strongly correlated with ISM variations and resulting CGT patterns.

Analysis of group SST differences showed EP La Niña and a strong warm anomaly appeared in the seas around Korea and Japan, which we attributed to increased solar radiation because precipitation decreased due to a strong anomalous anticyclone. This strong warm anomaly in the sea near Korea increased the discomfort index by providing additional heat and humidity in coastal areas.

We selected the years with the highest and lowest HWD frequencies in the HWD time series and analyzed in these two cases. The years with the highest and lowest HWD frequencies in the HWD time series were 2018 and 1993, respectively. To examine the unique characteristics of these two years, differences between these two years and climatology was analyzed. The results for Air2m, precipitation, SST, 200 hPa stream flows, and TC tracks in 2018 were similar to the analyses obtained from the difference between the two groups, and the results for 1993 showed the opposite pf the case in 2018.

Declarations

Acknowledgements

This work was carried out with the support of "Cooperative Research Program for Agriculture Science & Technology Development (Project No. PJ01489102)" Rural Development Administration, Republic of Korea

References

Adler RF, Huffman GJ, Chang A, Ferraro R, Xie P, Janowiak J, Rudolf B, Schneider U, Curtis S, Bolvin D, Gruber A, Susskind J, Arkin P, Nelkin E (2003) The Version-2 Global Precipitation Climatology Project (GPCP) Monthly Precipitation Analysis (1979-Present). J Hydrometeorol 4:1147-1167

Anderson BG, Bell ML (2009) Weather-related mortality: How heat, cold, and heat waves affect mortality in the United States. Epid 20: 205-213

Byun HR, Hwang HS, Go HY (2006) Characteristics and synoptic causes on the abnormal heat occurred at Miryang in 2004. Atmosphere 16: 187-201 (in Korean with English abstract).

Choi BC, Kim J, Lee DG, Kysely J (2007) Long-term trends of daily maximum and minimum temperatures for the major cities of South Korea and their implications on human health. Atmosphere 17: 171-183 (in Korean with English abstract).

Ding Q, Wang B (2005) Circumglobal teleconnection in the Northern Hemisphere Summer. J Clim 18: 3483-3505

Ding Q, Wanf B, Wallace JM, Branstator G (2011) Tropical-extratropical teleconnections in boreal summer: Observed interannual variability. J Clim 24: 1878-1896, doi:10.1175/2011JCLI3621.1

Fink AH, Brücher T, Krüger A, Leckebusch GC, Pinto JG, Ulbrich U (2004) The 2003 European summer heatwaves and drought–synoptic diagnosis and impacts. Weather 59: 209-216

Garcia-Herrera R, Diaz J, Trigo RM, Luterbacher J, Fischer EM (2010) A review of the European Summer heat wave of 2003. Crit Rev Environ Sci Tech 40: 267-306

Ha KJ, Seo YW, Lee JY, Kripalani RH, Yun KS (2018) Linkages between the South and East Asian summer monsoons: a review and revisit. Clim Dyn 51: 4207-4227, doi:10.1007/s00382-017- 3773-z.

Ha KJ, Ha EH, Yoo CS, Jeon EH (2004) Temperature trends and extreme climate since 1909 at big four cities of Korea. Asia-Pac J Atmos Sci 40: 1-16 (in Korean with English abstract)

Hsu PC, Lee JY, Ha KJ (2016) Influence of boreal summer intraseasonal oscillation on rainfall extremes in southern China. Int J Climatol 36: 1403-1412, doi:10.1002/joc.4433.

Hsu PC, Lee JY, Ha KJ, Tsou CH (2017) Influences of boreal summer intraseasonal oscillation on heat waves in Monsoon Asia. J Clim 30: 7191- 7211, doi:10.1175/JCLI-D-16-0505.1.

Hulme M, Zhao ZC, Jiang T (1994) Recent and future climate change in East Asia. Inter J Climatol 14: 637-658.

IPCC. 2013: Summary for Policymakers. In: Climate Change 2013, The Physical Science Basis. Contribution of Working Group I to the Fifth Assessment Report of the Intergovernmental Panel on Climate Change [Stocker TF, Qin D, Plattner G-K, Tignor M, Allen SK, Boschung J, Nauels A, Xia Y, Bex V, Midgley PM (eds.)]. Cambridge University Press, Cambridge, United Kingdom and New York, NY, USA

Kalnay E, Kanamitsu M, Kistler R et al (1996) The NCEP/NCAT 40-year reanalysis project. Bull Am Meteorol Soc 77:437-471

Kim HG, Min KD, Yoon IH, Moon YS, Lee DI (1998) Characteristics of the extraordinary high temperature events occurred in Summers of 1987 and 1994 over the Korean Peninsula. Asia-Pac J Atmos Sci 34: 47-64 (in Korean with English abstract).

Kim JA, Kim KR, Lee CC, Sheridan SC, Kalkstein LS, Kim BJ (2016) Analysis of occurrence distribution and synoptic pattern of future heat waves in Korea. J Clim Res 11: 15-27 (in Korean with English abstract)

Kim YS, Hong SK (1996) A study of quasi-Foehn in the Youngdong-district in late spring of early Summer. Asia Pac J Atmos Sci 32: 593-600 (in Korean with English abstract).

Klinenberg E (1999) Denaturalizing disaster: A social autopsy of the 1995 Chicago heat wave. Theory and Society 28: 239-295

Knowlton K, Rotkin-Ellman M, King G, Margolis HG, Smith D, Solomon G, Trent R, English P (2009) The 2006 California heat wave: Impacts on hospitalization and emergency department visits. Envir Heal Persp 117: 61-67

Kysely J, Kim J (2009) Mortality during heat waves in South Korea, 1991 to 2005: How exceptional was the 1994 heat wave? Clim Res 38: 105-116.

Lee DK, Park JG (1999) Regionalization of summer rainfall in South Korea using cluster analysis. Asia-Pac J Atmos Sci 35: 511-518 (in Korean with English abstract).

Lee JY (2018) Interdecadal changes in the boreal summer tropical-extratropical teleconnections occurred around mid-to-late 1990s. Atmosphere 28: 325-336, doi:10.14191/Atmos.2018.28.3.325 (in Korean with English abstract).

Lee JY, Ha KJ (2015) Understanding of interdecadal changes in variability and predictability of the Northern Hemisphere summer tropical-extratropical teleconnection. J Clim 23: 8634-8647, doi: 10.1175/JCLI-D-15-0154.1.

Lee JY, B Wang, Q Ding, Ha KJ, Ahn JB, Kumar A, Stern B, Alves O (2011) How predictable is the Northern Hemisphere summer upper-tropospheric circulation? Clim Dyn 37: 1189-1203, doi:10.1007/ s00382-010-0909-9.

Lee JY, Hsu PC, Moon S, Ha KJ (2017a) Influence of boreal summer intraseasonal oscillation on Korean precipitation and its long-term changes. Atmosphere 27: 435-444, doi:10.14191/Atmos.2017.27.4.435 (in Korean with English abstract).

Lee JY, Kim HJ, Jeong YR (2019) Influence of boreal summer intraseasonal oscillation on the 2016 heat wave over Korea (in Korean with English abstract)

Lee JY, Coauthors (2017b) The long-term variability of Changma in the East Asian summer monsoon system: A review and revisit. Asia-Pac J Atmos Sci 53: 257-272, doi:10.1007/s13143-017-0032-5.

Li JP, Zeng QC (2002) A unified monsoon index. Geophys Res Lett 29:1274, doi:10.1029/2001GL013874

Li JP, Zeng QC (2003) A new monsoon index and the geographical distribution of the global monsoons. Adv Atmos Sci 20:299-302

Li JP, Zeng QC (2005) A new monsoon index, its interannual variability and relation with monsoon precipitation. Climatic and Environmental Research 10:351-365

Meehl GA, Tebaldi C (2004) More intense, more frequent, and longer lasting heat waves in the 21st century. Sci 305: 994-997.

Robine JM, Cheung SLK, Roy SL, Oyen HV, Griffiths C, Micheal JP, Herrmann FR (2008) Death toll exceeded 70,000 in Europe during the summer of 2003. Comp Rend Biolo 331: 171-178

Schär C, Vidale PL, Lüthi D, Frei C, Häberli C, Liniger MA, Appenzeller C (2004) The role of increasing temperature variability in European summer heatwaves. Nature 427: 332-336

Semenza JC, Rubin CH, Falter KH, Selanikio JD, Flanders WD, Howe HL, Wilhelm JL (1996) Heat-related deaths during the July 1995 heat wave in Chicago. The New Eng J Medic 335: 84-90.

Smith TM, Reynolds RW, Peterson TC, Lawrimore J (2008) Improvements to NOAA's historical merged Land-Ocean surface temperature analysis (1880-2006). J Clim 21:2283-2296

Wei W, Zhang R, Wen M (2012) Meridional variation of South Asian High and its relationship with the summer precipitation over China. J Appl Meteorol Sci 23:650-659 (in Chinese)

Wei W, Zhang R, Wen M, Rong X, Li T (2014) Impact of Indian summer monsoon on the South Asian High and its influence on summer rainfall over China. Clim Dyn 43:1257-1269

Yeh SW, Won YJ, Hong JS, Lee KJ, Kwon M, Seo KH, Ham YG (2018) The record-breaking heat wave in 2016 over South Korea and its physical mechanism. Mon Wea Rev 146: 1463-1474, doi:10.1175/MWR-D-17-0205.1

Yeo, SR, Yeh SW, Lee WS (2019) Two types of heat wave in Korea associated with atmospheric circulation pattern. J Geophy Res-Atmos 124: 7498-7511

Figures

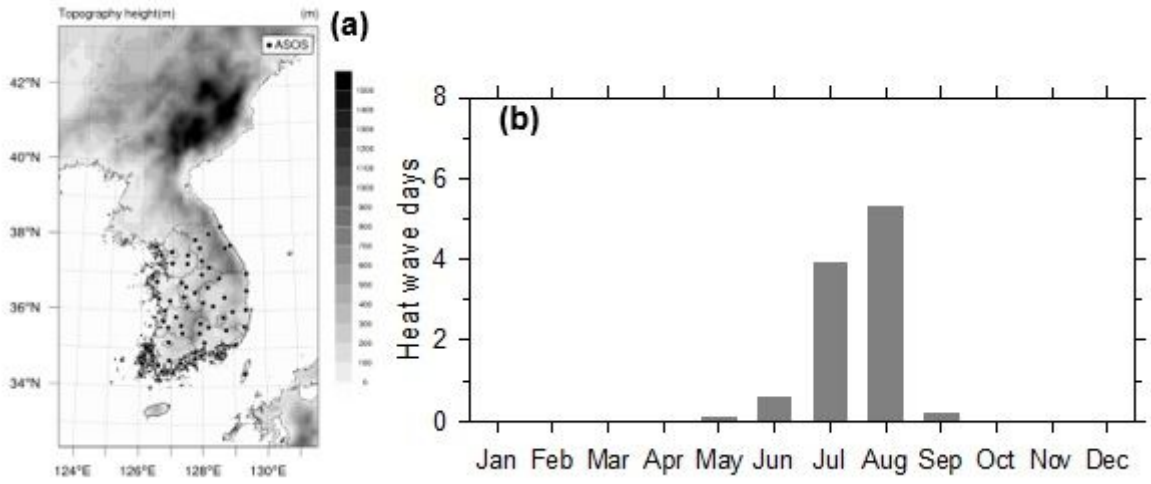

Figure 1

(a) spatial distribution of weather observation station in Korea and (b) monthly distribution of heat wave days (HWD).

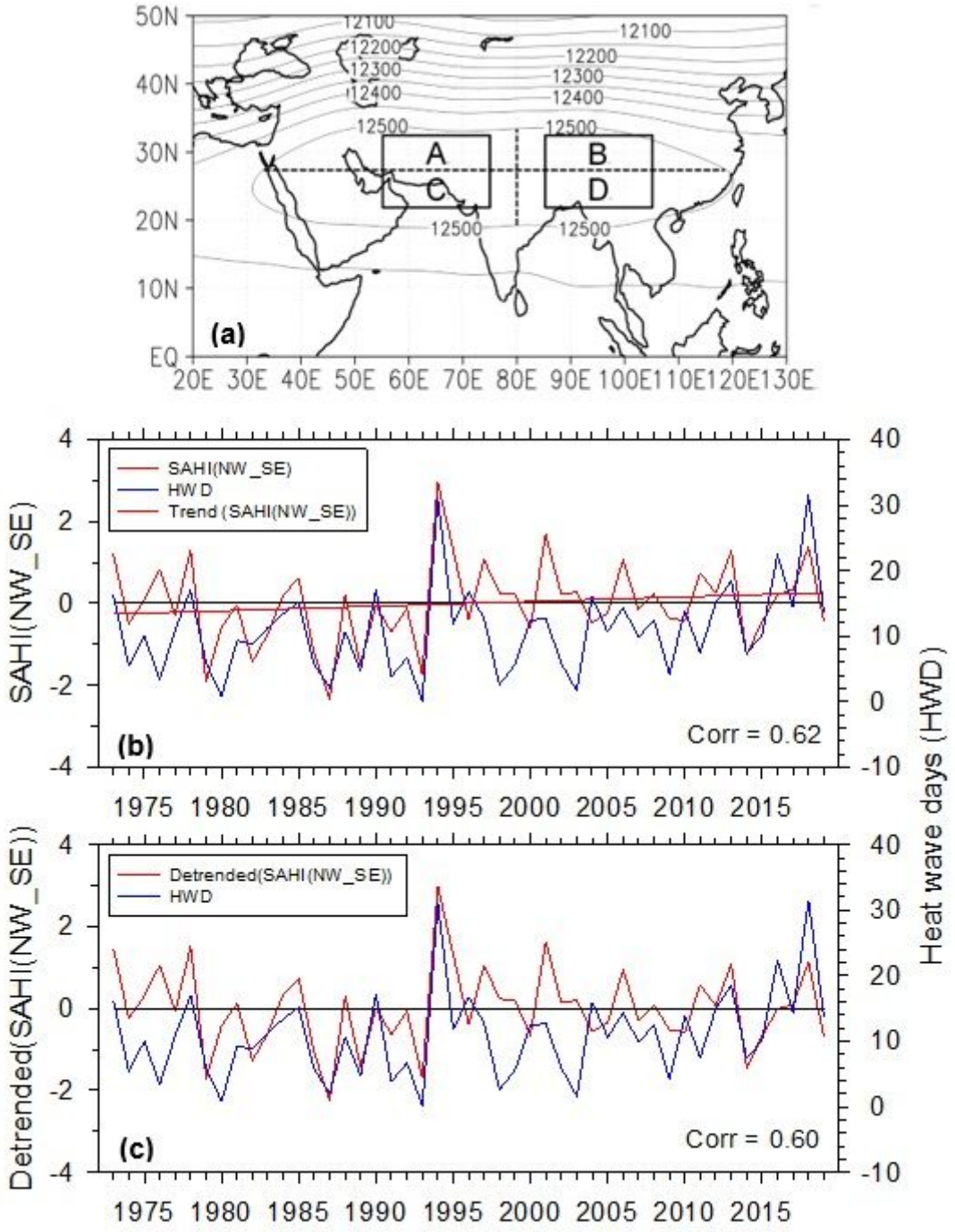

Figure 2

(a) July-August (JA) climatological mean 200 hPa geopotential height and time series of (b) South Asian high (SAH) index (A area minus D area in (a)) and HWD in Korea and (c) detrended SAH index and HWD in Korea. In (a) A, B, C and D denote northwestern (NW), northeastern (NE), southwestern (SW) and southeastern areas of SAH.

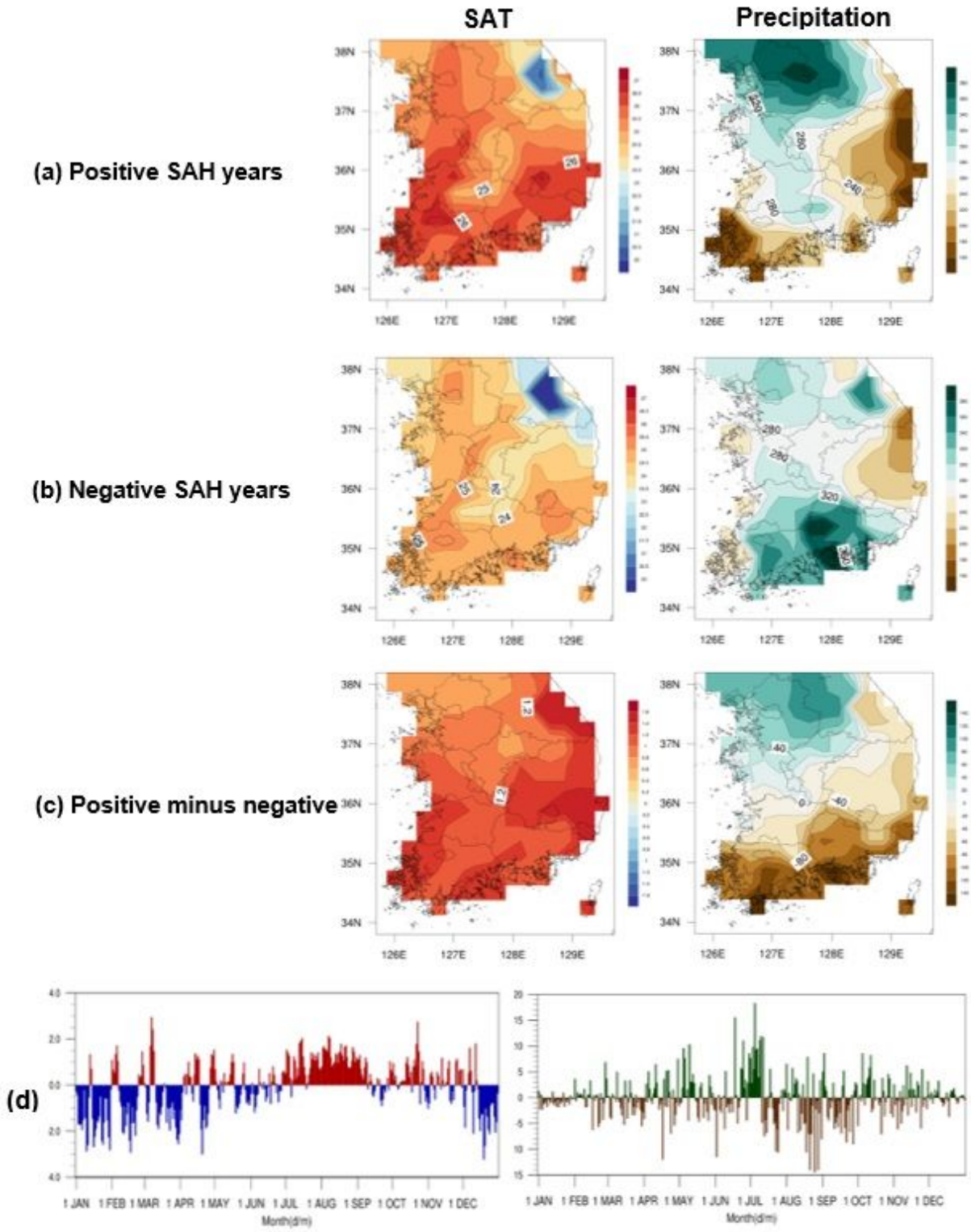

Figure 3

Spatial distributions of surface air temperature (SAT; °C) (left panel) and precipitation (mm) (right panel) in (a) positive SAH years, (b) negative SAH years, and (c) positive minus negative SAH years in JA. (d) Daily time series of SAT (°C) (left panel) and precipitation (mm) (right panel) in positive minus negative SAH years.

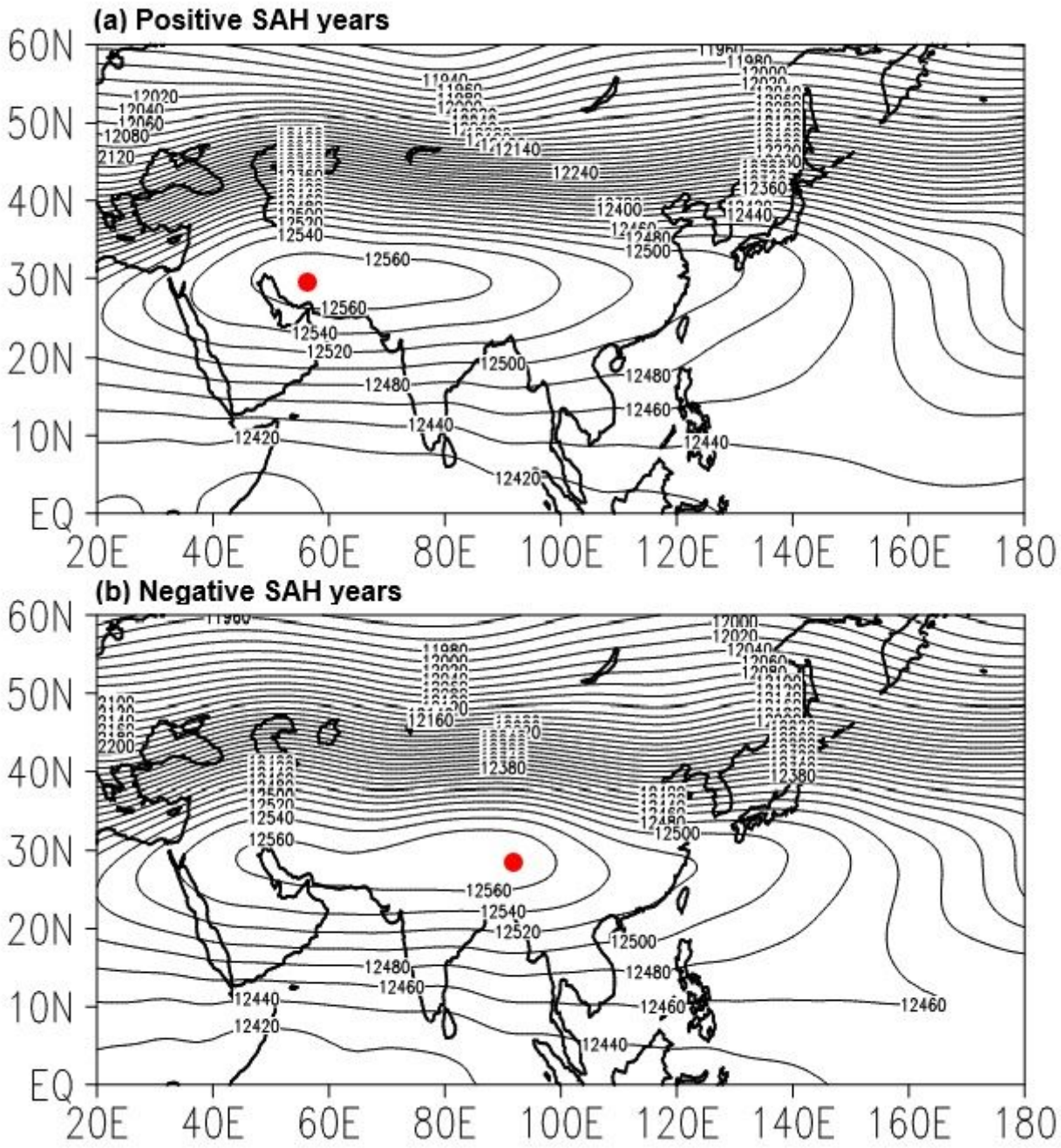

Figure 4

JA mean 200 hPa geopotential height (a) in positive SAH years and (b) in negative SAH years. Red dots denote centers of SAH.

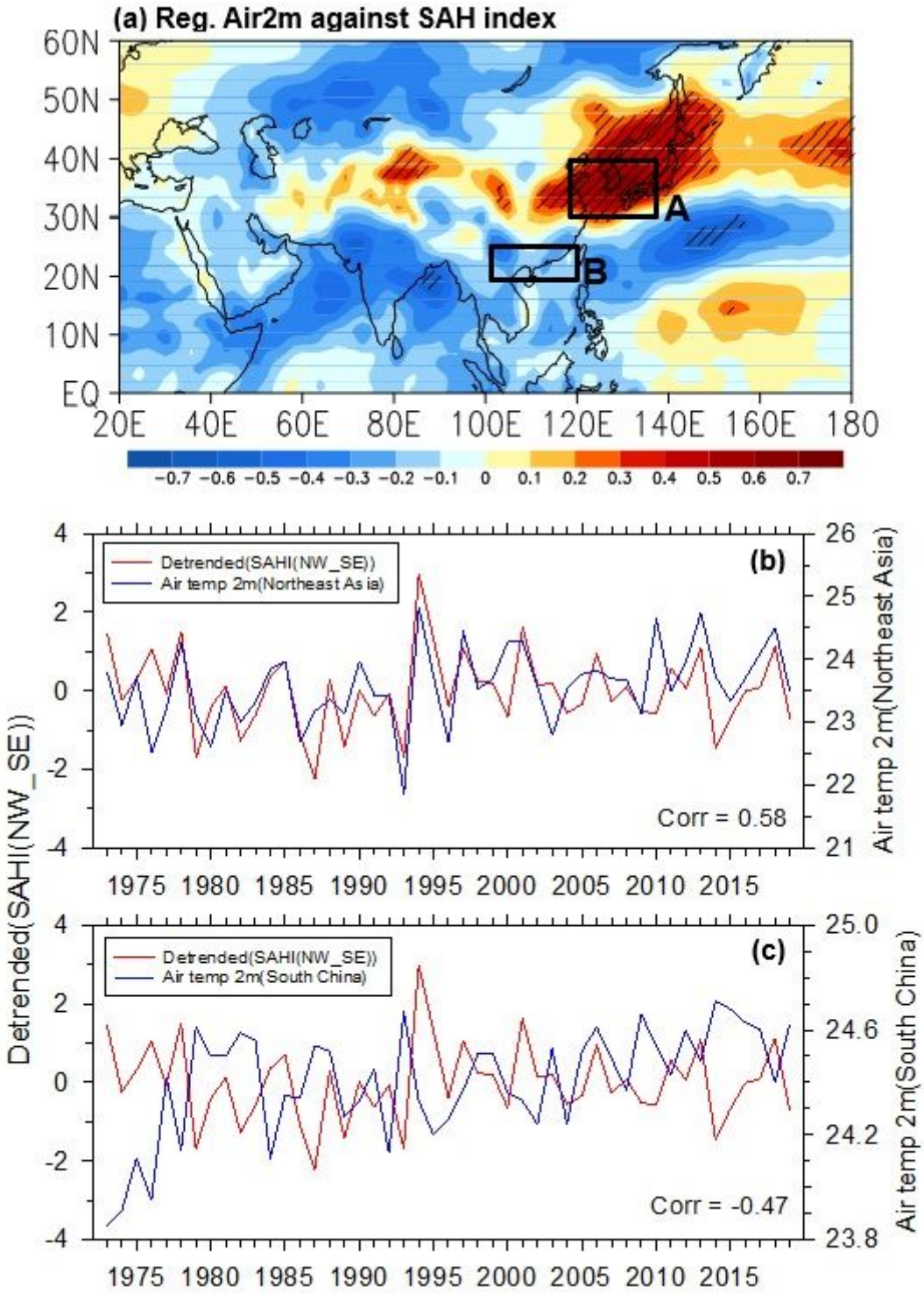

Figure 5

(a) regression map of 2m air temperature (Air2m) against SAH index in JA and time series of SAH index and Air2m in (b) Northeast Asia (A area: 30°-40°N, 120°-140°E) and (c) South China (B area: 20°-25°N, 100°-120°E).

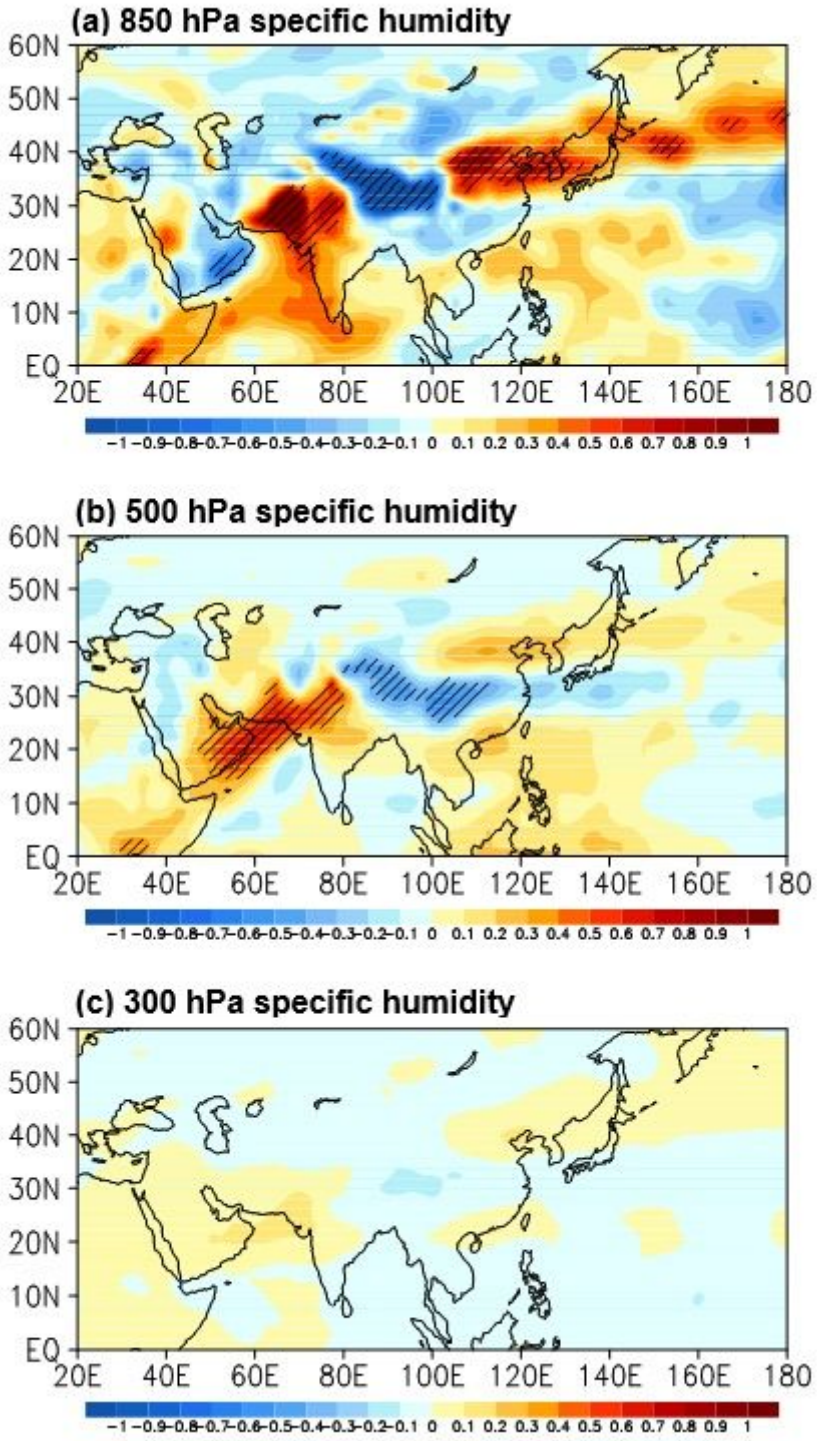

Figure 6

Composite differences in (a) 850, (b) 500 and (c) 300 hPa specific humidity between positive SAH years and negative SAH years in JA. Hatched areas are significant at the 95% confidence level.

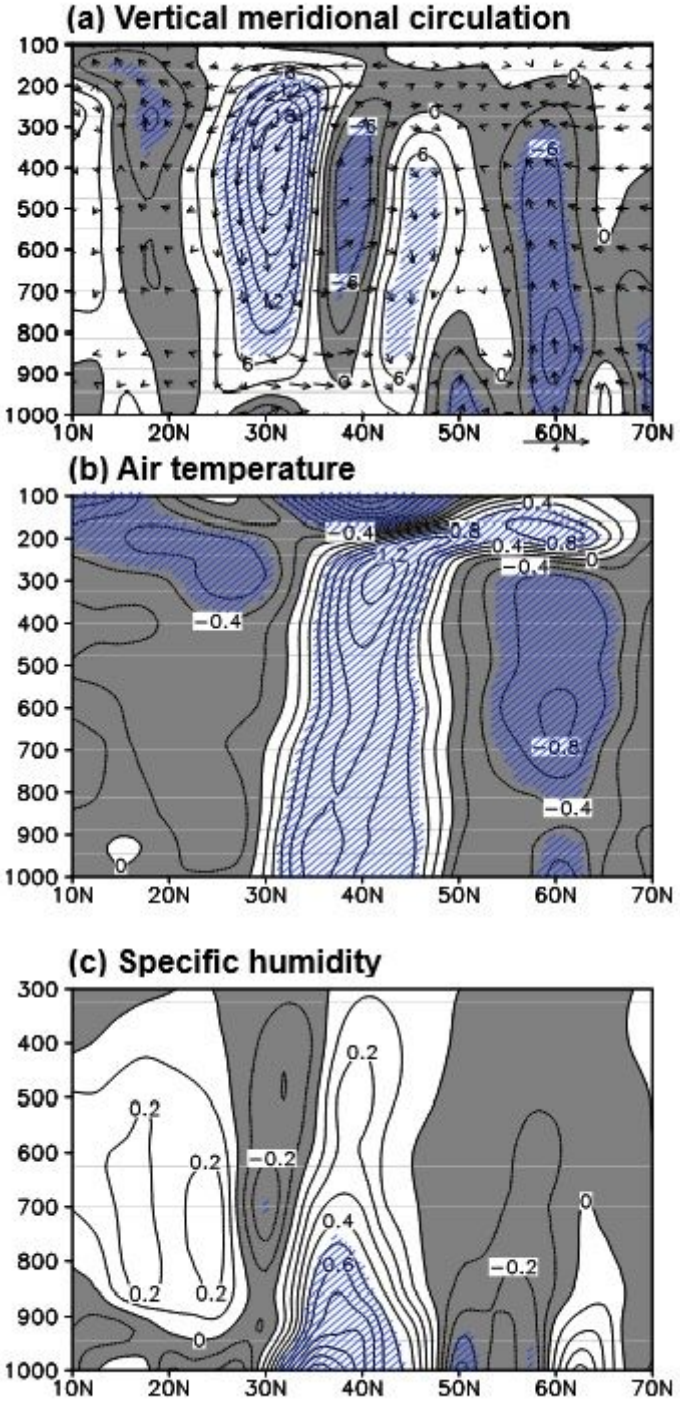

Figure 7

Composite differences of latitude–pressure cross-section of (a) vertical velocity (contours) and meridional circulations (vectors), (b) air temperature and (c) specific humidity averaged along 120°-130°E between positive and negative SAT years in JA. The values of vertical velocity are multiplied by −100. Dashed areas are significant at the 95% confidence level and shaded areas denote negative values. Contour intervals are 3−2hPa s−1, 0.2°C, and 0.1 g kg-1 for vertical velocity, air temperature and specific humidity, respectively.

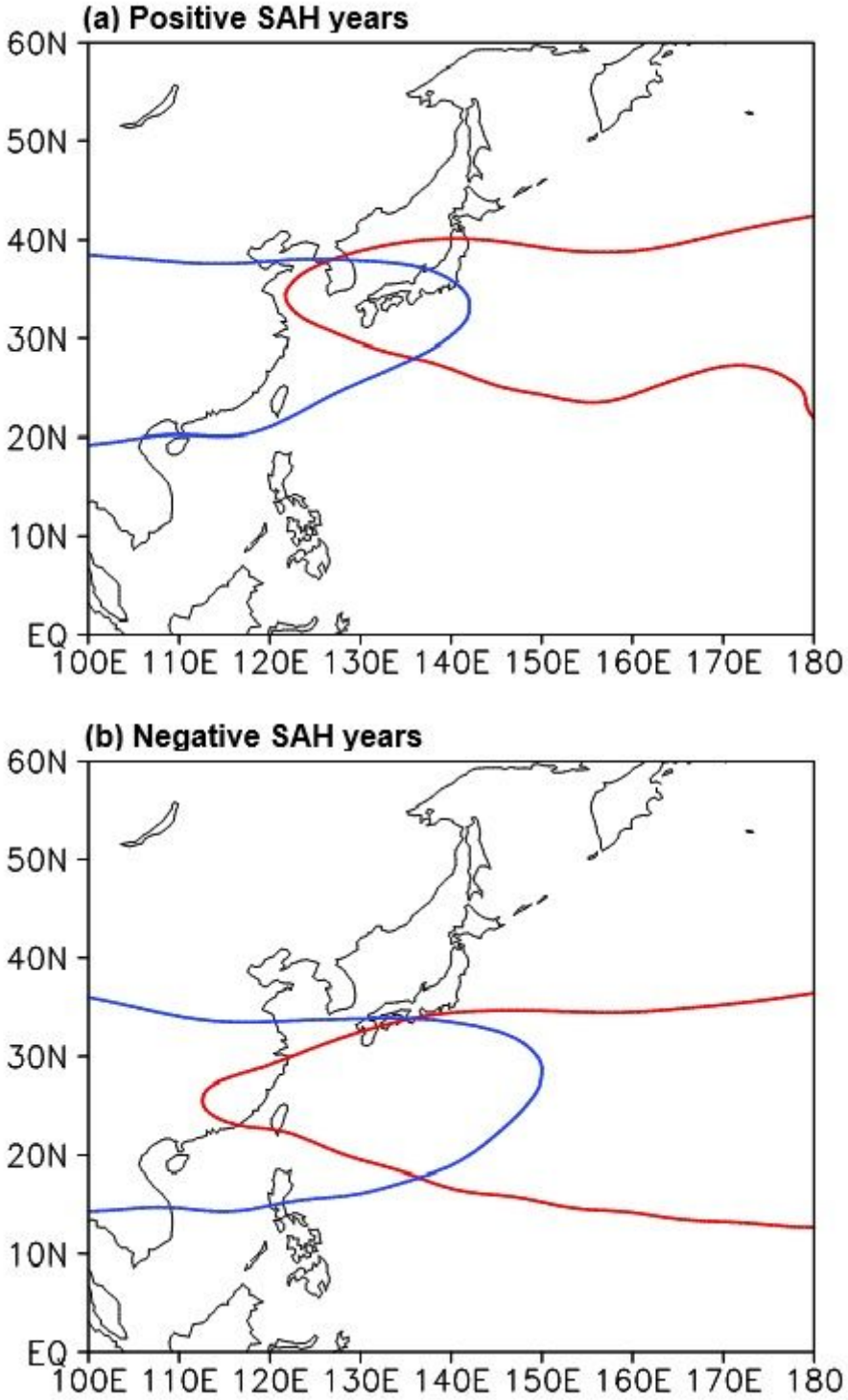

Figure 8

Spatial distributions of western North Pacific subtropical high (WNPSH; 5,870 gpm contour) and SAH (12,480 gpm contour) in JA. Red and blue lines indicate WNPSHs and SAHs in positive SAH years and negative SAH years, respectively.

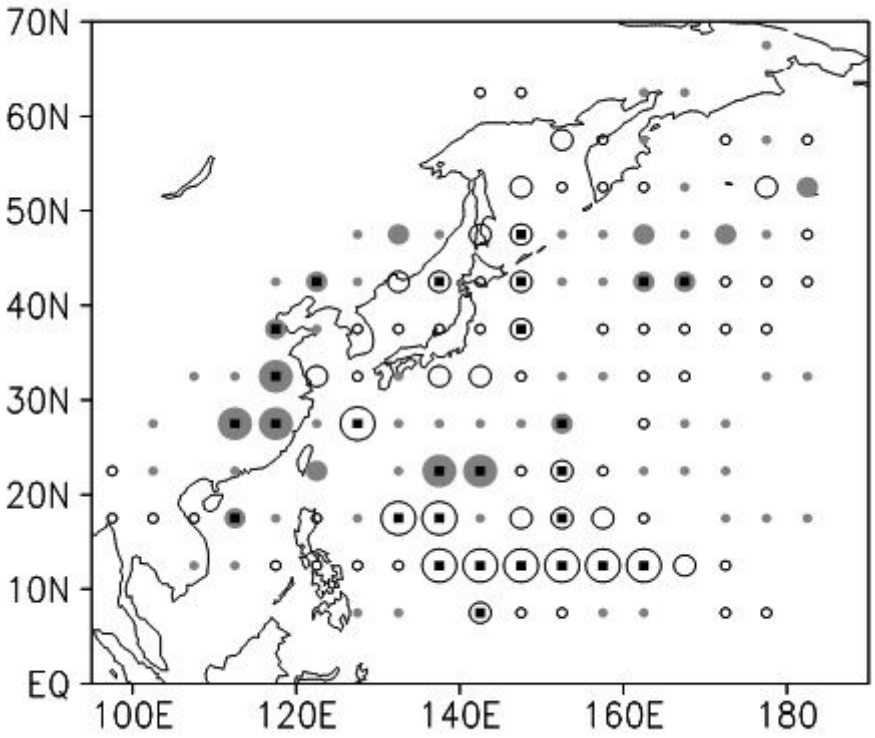

Figure 9

Composite difference in TC passage frequency (TCPF) between positive and negative SAH years in JA. Small squares inside the circles indicate that the differences are significant at the 95 % confidence level.

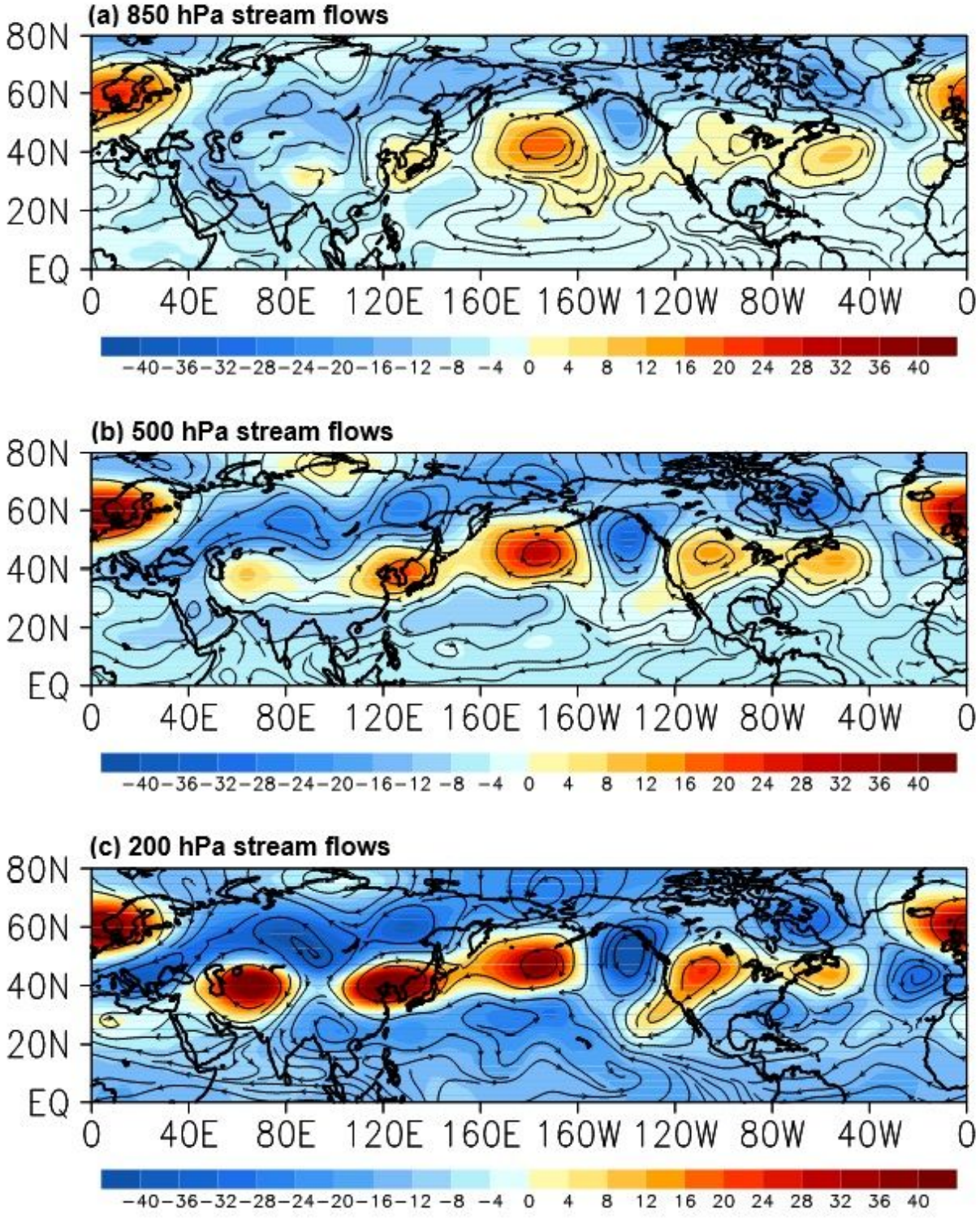

Figure 10

Composite differences in (a) 850 hPa, (b) 500 hPa and (c) 200 hPa stream flow and geopotential height between positive and negative SAH years in JA.

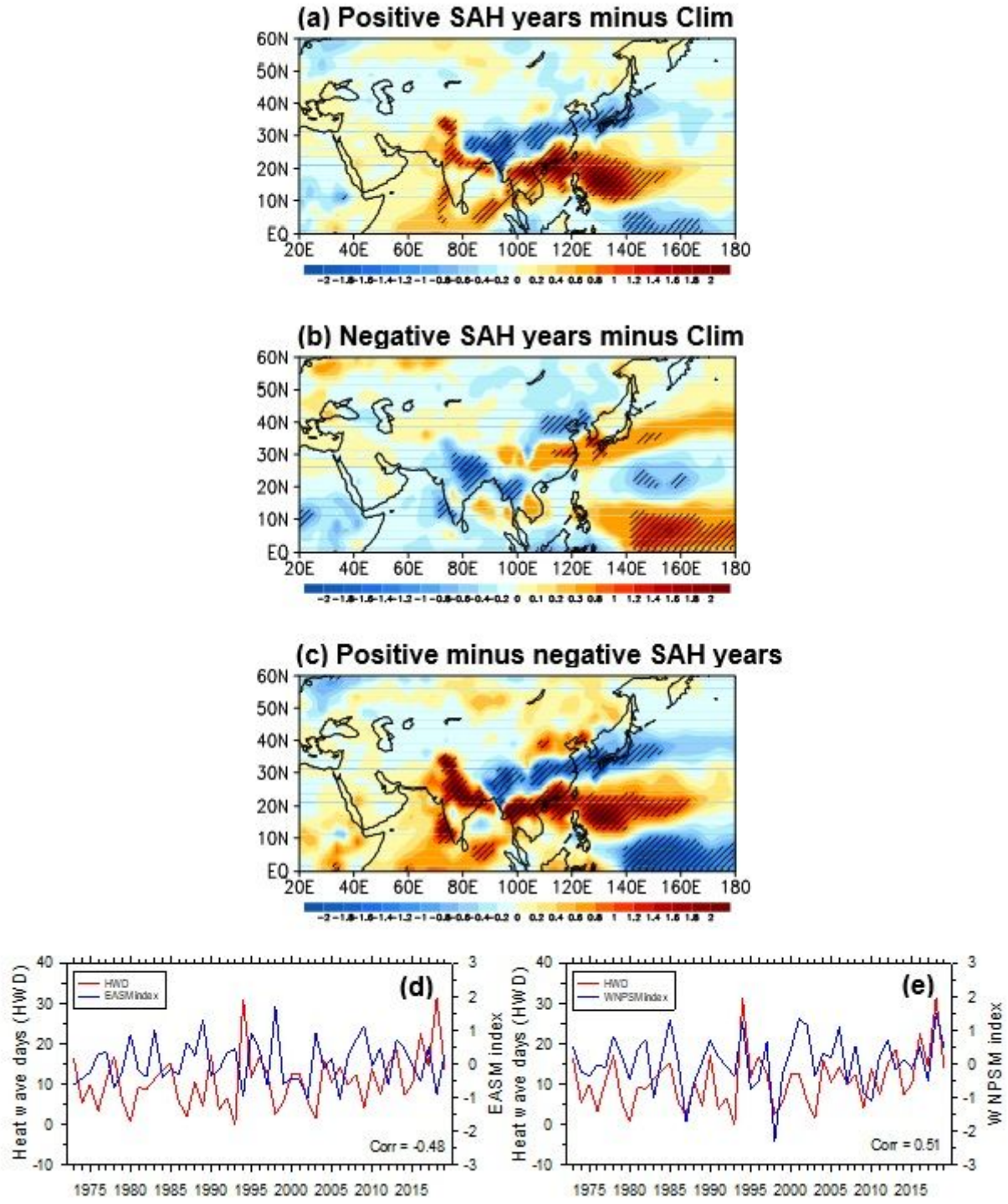

Figure 11

Differences in precipitation (a) between positive SAH years and climatology, (b) between negative SAH years and climatology and (c) between positive SAH years and negative SAH years in JA. Time series of (d) HWD in Korea and East Asian summer monsoon (EASM) index and (c) HWD in Korea and western North Pacific summer monsoon (WNPSM) index. Here, climatology indicates average from 1973 to 2019 in JA. In (a), (b) and (c), dashed areas are significant at the 95% confidence level.

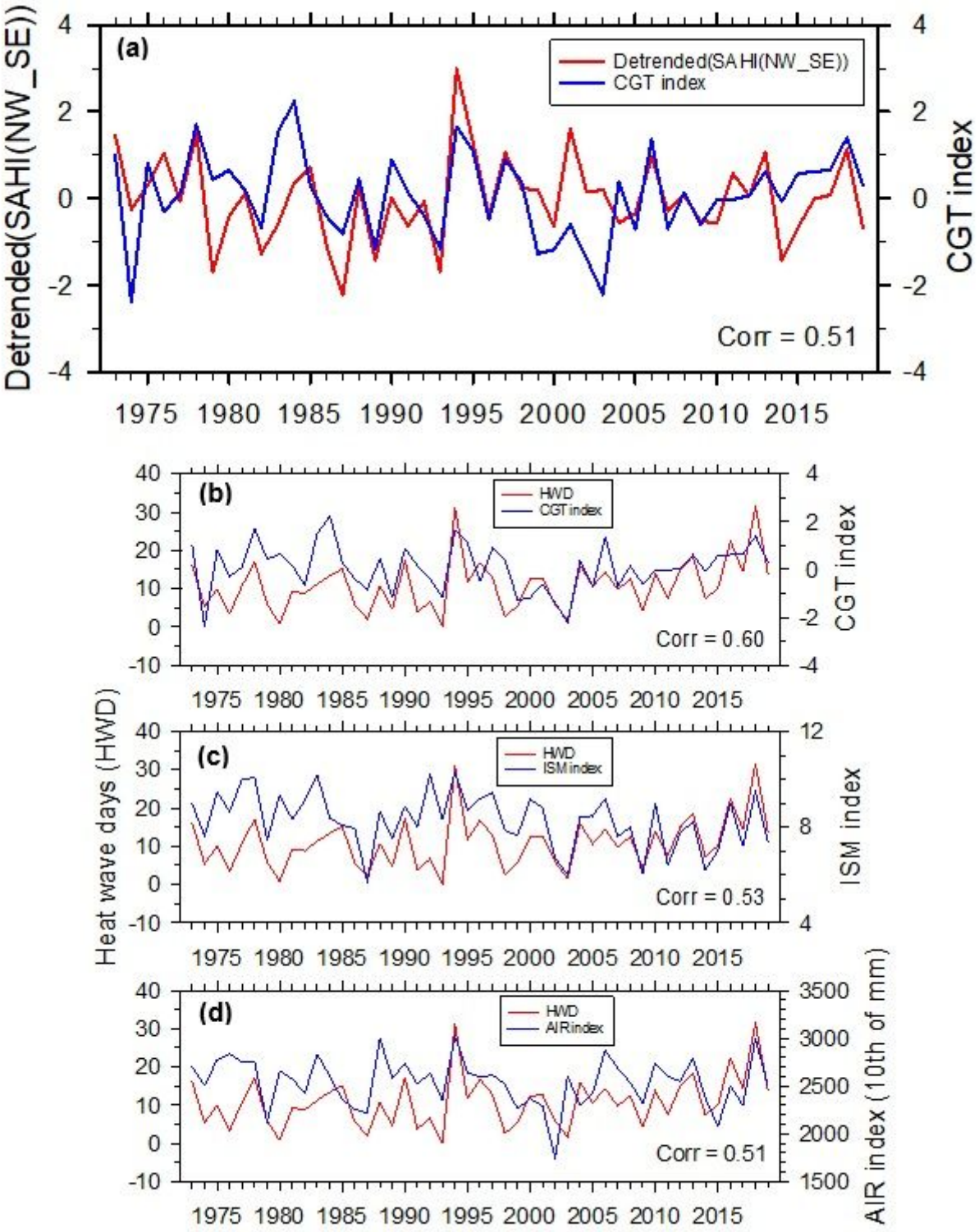

Figure 12

Time series of (a) SAH index and circumglobal teleconnection (CGT) index, (b) HWD in Korea and CGT index, (c) HWD in Korea and Indian summer monsoon (ISM) index and (d) HWD in Korea and all India rainfall (AIR) index in JA.

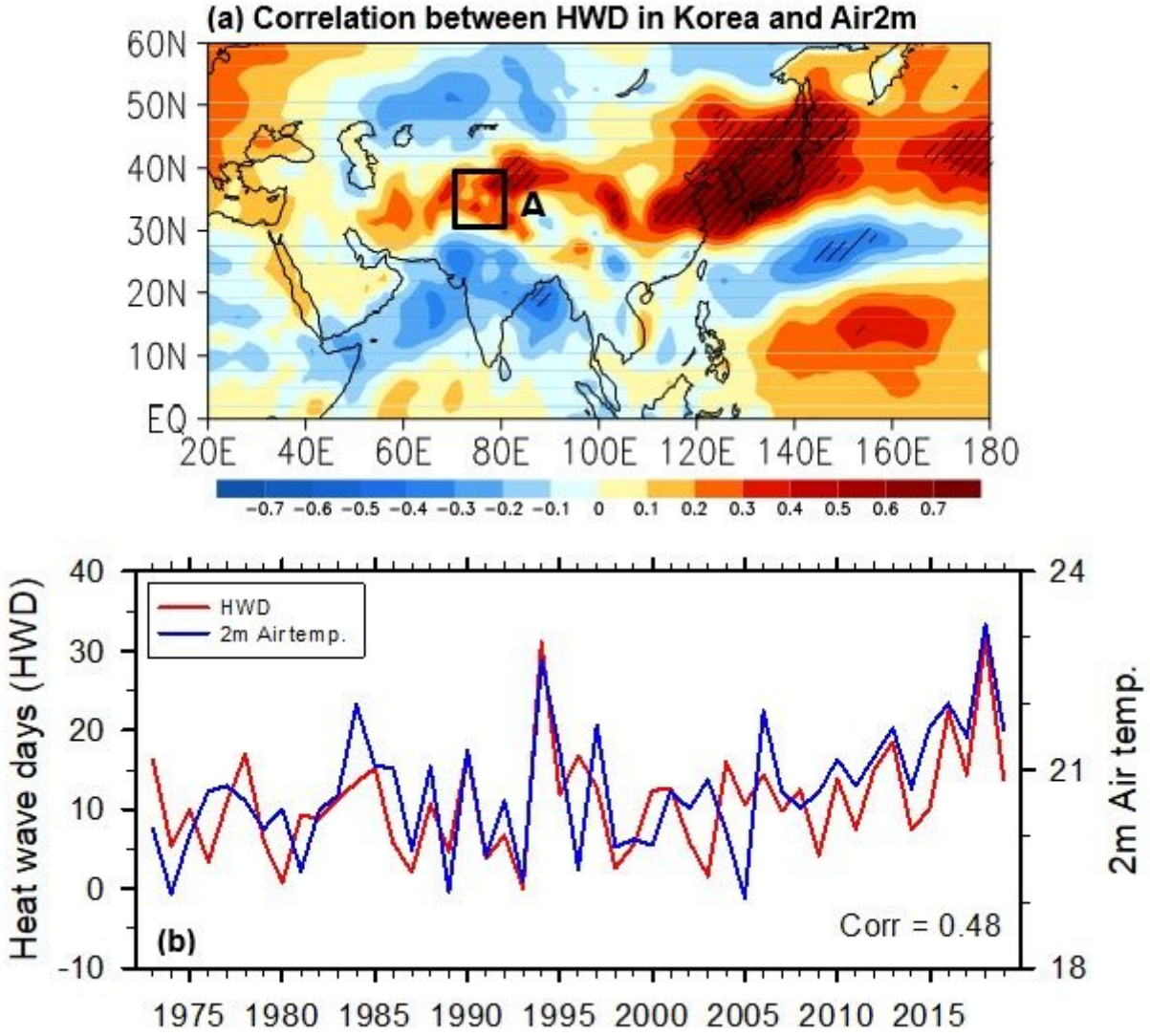

Figure 13

(a) Correlation map between HWD in Korea and Air2m in JA. (b) Time series of HWD in Korea and Air2m averaged over area A (30°-40°N, 70°-80°E) in (a). In (a), dashed areas are significant at the 95% confidence level.

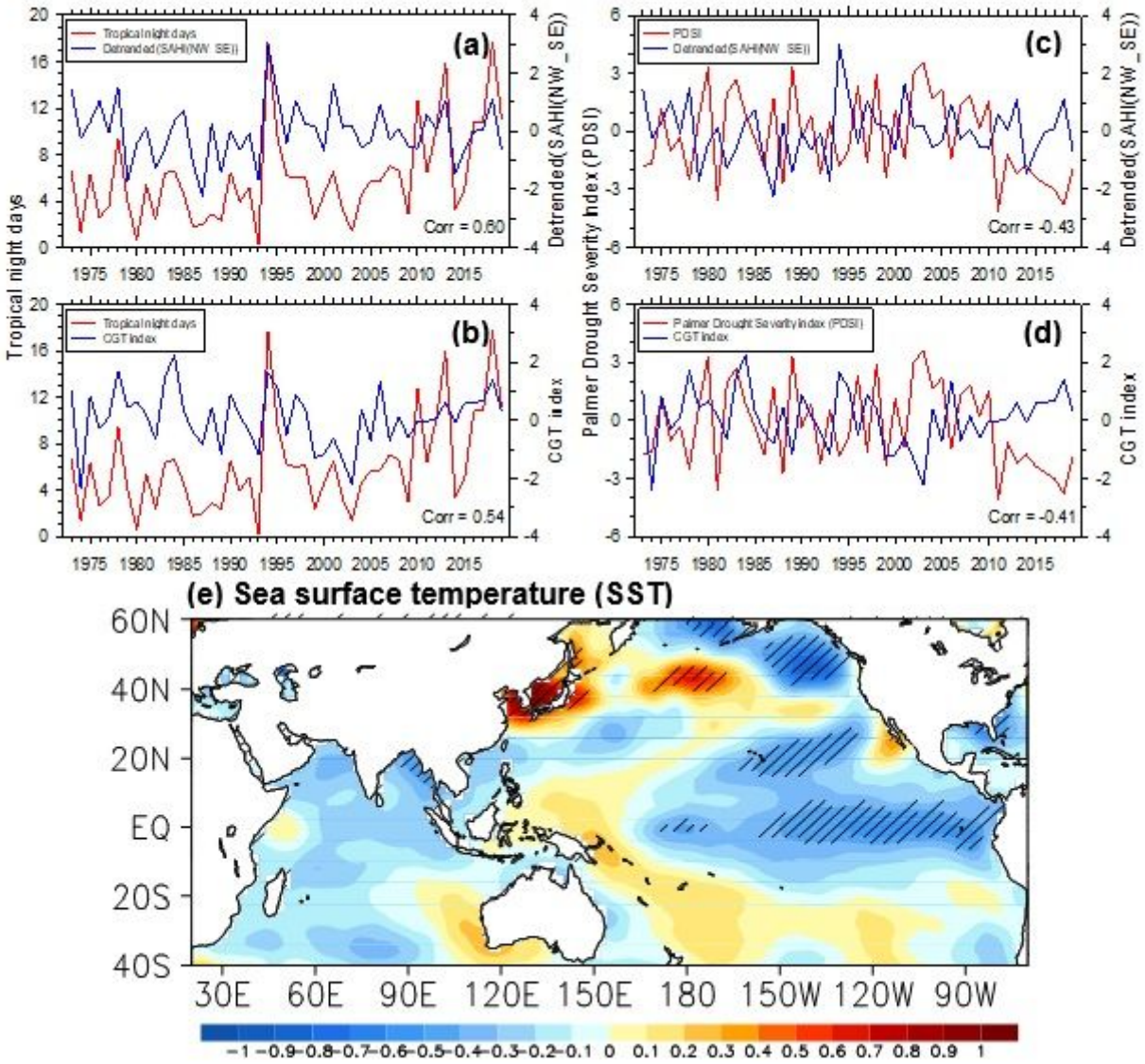

Figure 14

Time series of (a) tropical night days (TND) in Korea and SAH index, (b) TND in Korea and CGT index, (c) Palmer Drought Severity index (PDSI) in Korea and SAH index and (d) PDSI in Korea and CGT index. (e) Composite difference in SST between positive SAH years and negative SAH years. In (e), dashed areas are significant at the 95% confidence level.

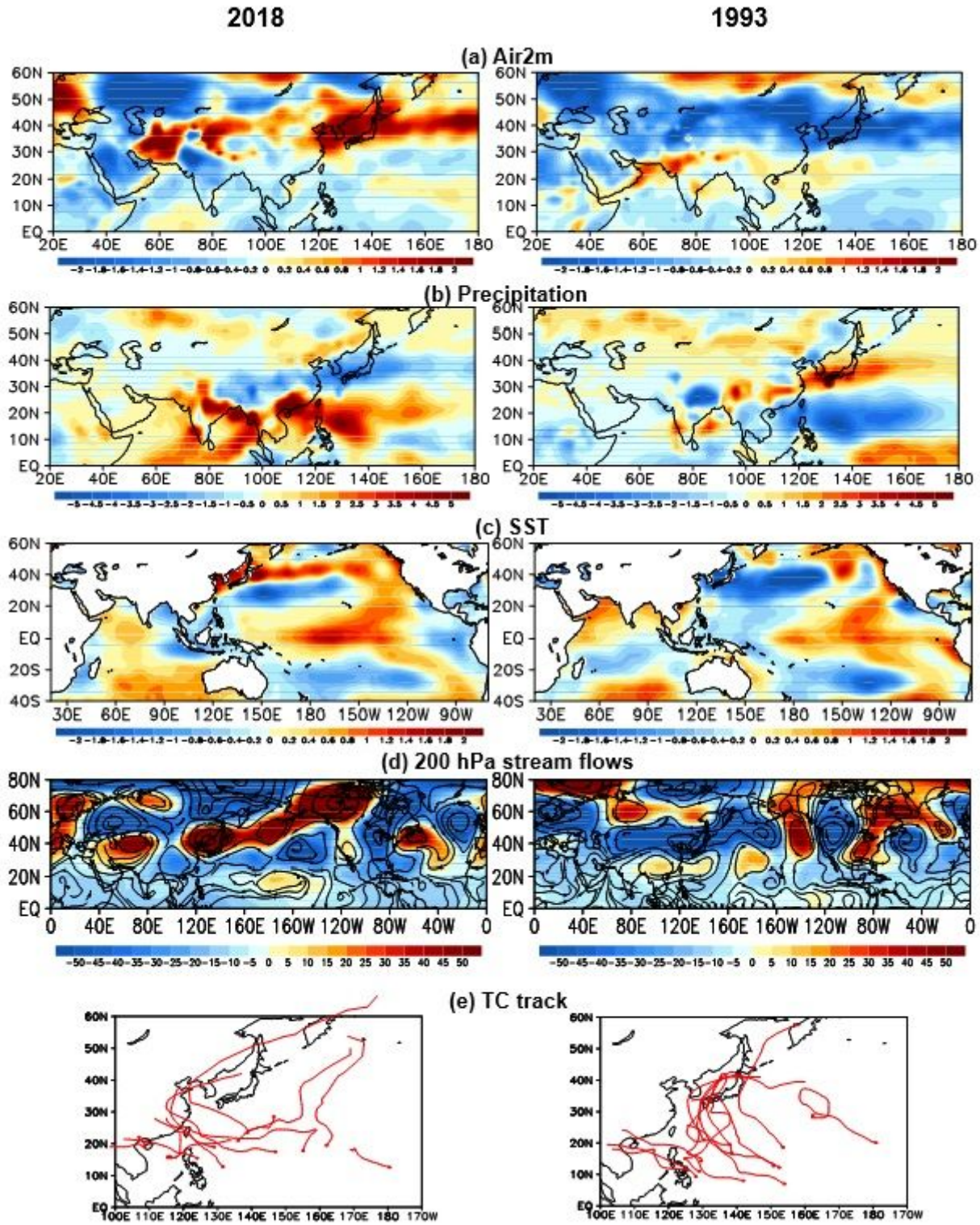

Figure 15

Differences in (a) Air2m, (b) precipitation, (c) SST and (d) 200 hPa stream flow and 200 hPa geopotential height between year of 2018 and climatology (left panel) and between year of 1993 and climatology (right panel). (e) TC tracks in 2018 (left panel) and in 1993 (right panel). Here, climatology indicates average from 1973 to 2019 in JA.

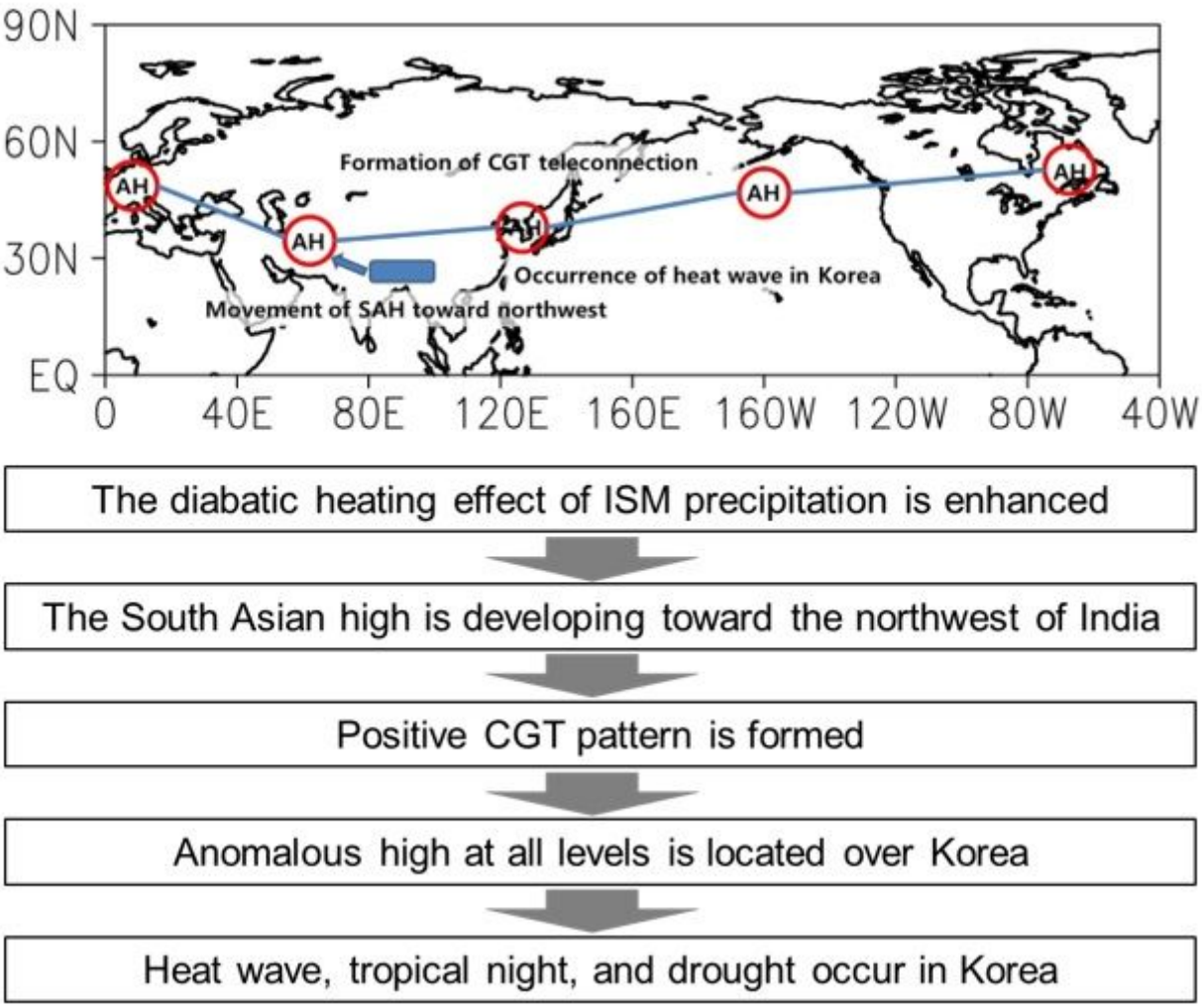

Figure 16

Schematic illustration of 200 hPa anomalous atmospheric circulations occurring during positive SAH years. “AH” indicates anomalous high.Note: The designations employed and the presentation of the material on this map do not imply the expression of any opinion whatsoever on the part of Research Square concerning the legal status of any country, territory, city or area or of its authorities, or concerning the delimitation of its frontiers or boundaries. This map has been provided by the authors.